Supporting Information

Asymmetric electrochemical system for chloride-mediated CO_2 removal from oceanwater

Seoni Kim[a], Michael P. Nitzsche[ab], Simon B. Rufer[b], Jack R. Lake[b],
Kripa K. Varanasi[b]* and T. Alan Hatton[a]*

[a]Department of Chemical Engineering, Massachusetts Institute of Technology, Cambridge, MA 02139, USA.

[b]Department of Mechanical Engineering, Massachusetts Institute of Technology, Cambridge, MA 02139, USA.

* Corresponding authors: tahatton@mit.edu, varanasi@mit.edu

S1. Experimental

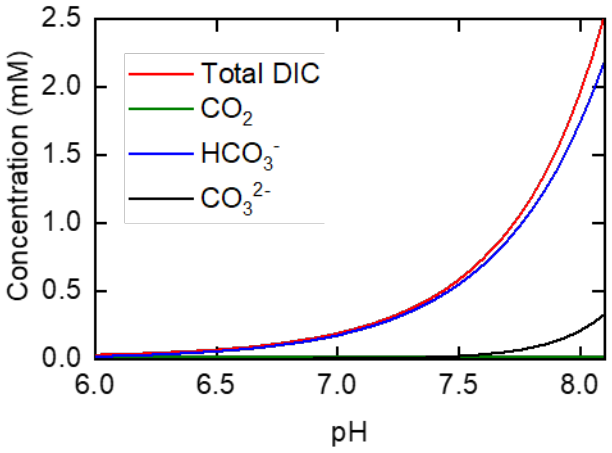

Fig. S1. Equilibrium concentration of inorganic carbon species and total DIC at pH 6-8.1 in simulated seawater calculated by assuming the activity coefficient of each species as unity.

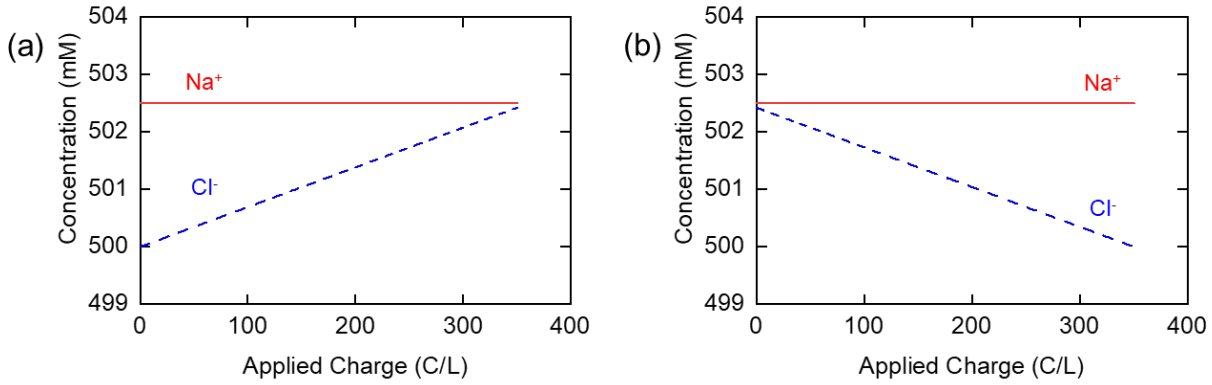

Fig. S2. Estimated equilibrium concentration of Na+ and Cl- (a) in pH decrease step and (b) in regeneration step.

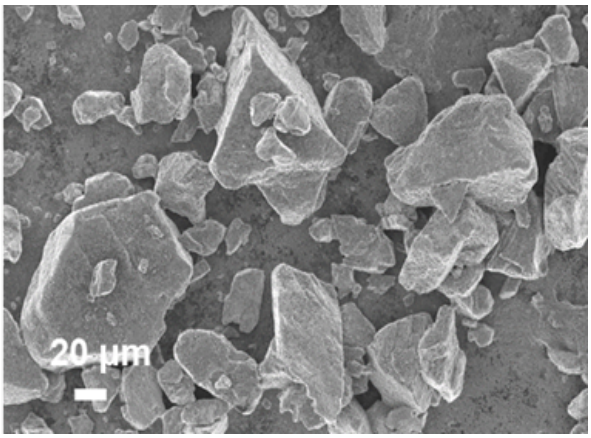

Fig. S3. SEM image of pristine bismuth particle before ball-mill.

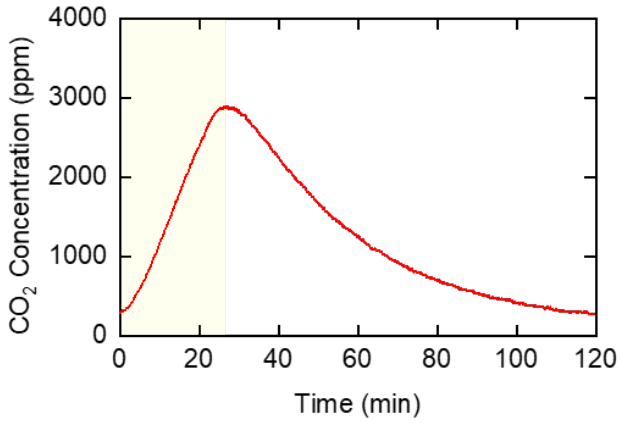

Fig. S4. CO_2 concentration measured at the headspace of a static cell for 120 minutes when –1 mA/cm^2 of current was applied in initial 25 minutes (yellow region).

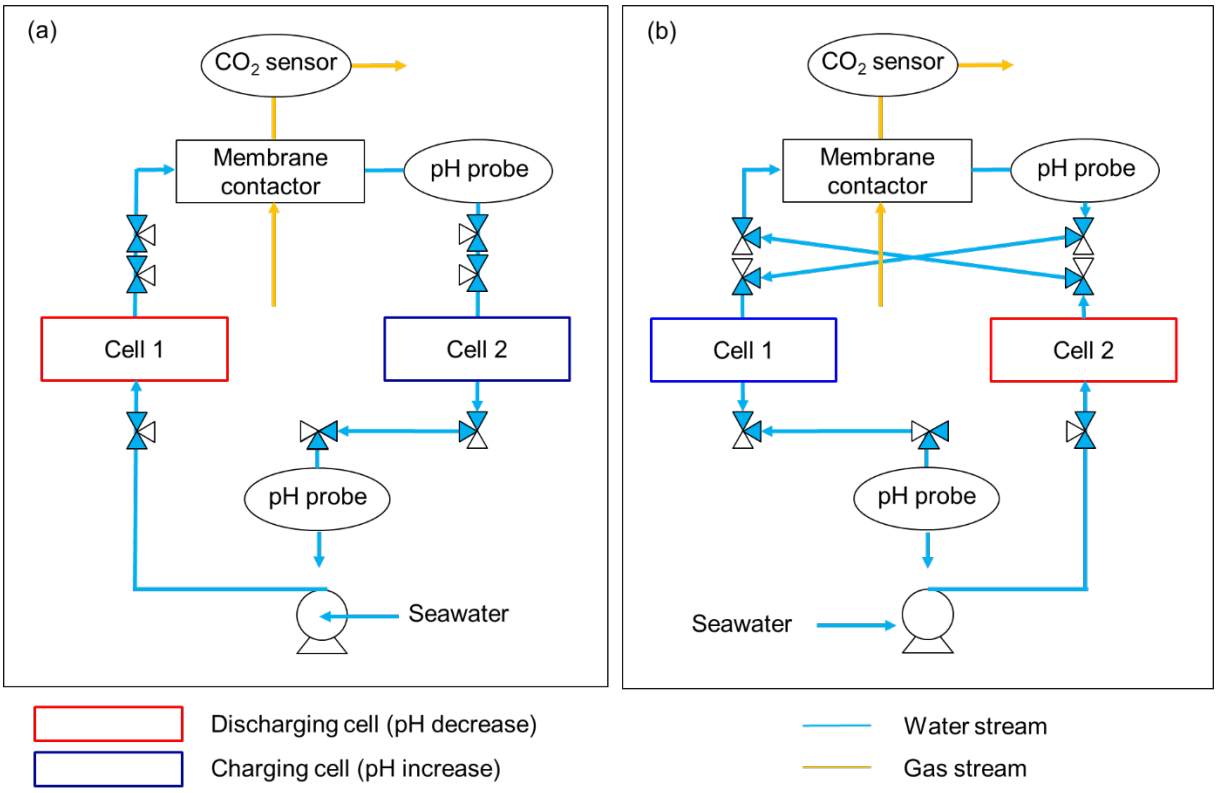

Fig. S5. Block diagram of continuous electrochemical pH-swing process for CO_2 removal from oceanwater. The process is operated by switching repetitively between (a) 1st step in which the pH decreases in Cell 1 and increases in Cell2 and (b) the 2nd step in which the pH decreases in Cell 2 and increases at Cell 1.

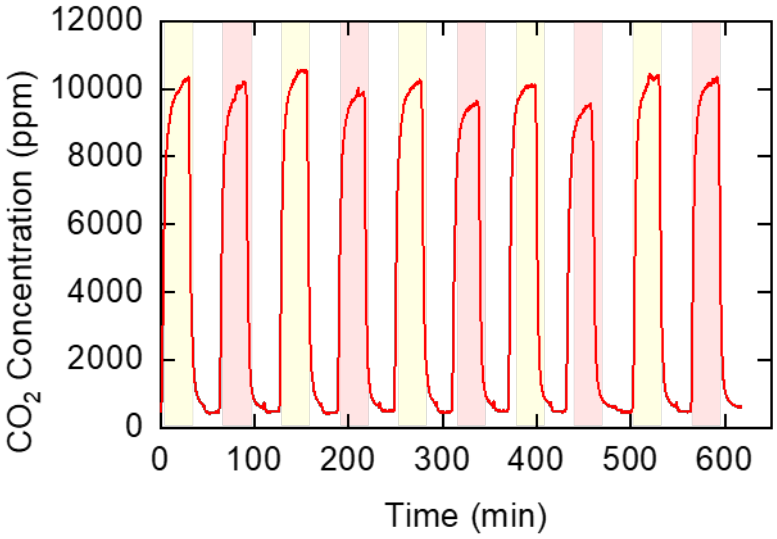

Fig. S6. CO_2 concentration profile monitored during the continuous electrochemical pH swing process operation for 10 cycles.

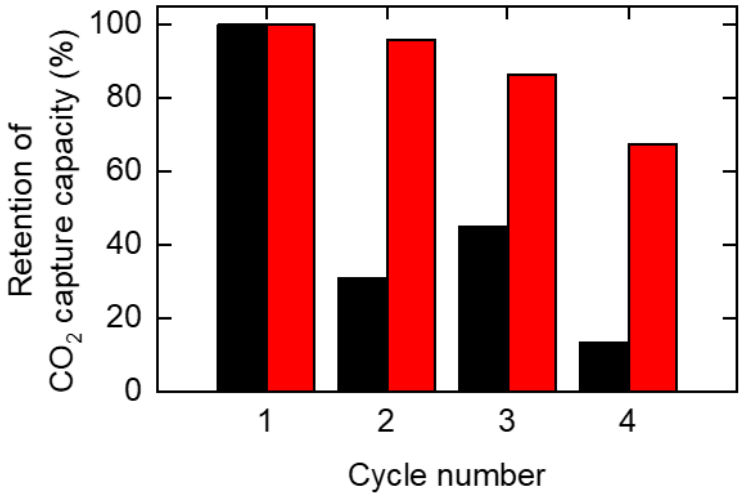

Fig. S7. Retention of CO_2 capture capacity of the electrochemical system using synthetic seawater (same composition as seawater) in 4-cycle operation at 1 mA/cm^2 (black) and 0.125 mA/cm^2 (red) of current density during the regeneration step.

S2. COMSOL Numerical Simulation

The numerical simulation was conducted using finite element analysis in COMSOL Multiphysics 6.0, coupling the Nernst-Planck equations in an aqueous electrolyte with laminar flow in a time-dependent solver.

Bulk equilibrium reactions were implemented as pointwise rate laws of the form:

$$\frac{dc_i}{dt} = \sum_j (k^*_{j,\rightarrow} \prod_l c_l{}^{\nu_l} - k^*_{j,\leftarrow} \prod_l c_l{}^{\nu_l}) \quad \text{(S1)}$$

c_i represents the concentration of a given species, $k^*_{j\leftrightarrow}$ are the forward and reverse rate constants for a given equilibrium reaction accounting for deviations from ideal activity, and ν represents the corresponding positive stoichiometric coefficient. Equilibrium reactions and rate constants are tabulated below, as formulated by Zeebe et. al (assuming T=25C, P=1 bar, and total salinity S=25 g/kg):

Reaction	pK^*	$k^*_{\rightarrow}$	$k^*_{\leftarrow}$
$CO_2 + H_2O \rightleftarrows HCO_3^- + H^+$	5.86	3.71×10^{-2} [s^{-1}]	2.58×10^{4} [$M^{-1}s^{-1}$]
$CO_2 + OH^- \rightleftarrows HCO_3^-$	/	3.91×10^{3} [$M^{-1}s^{-1}$]	1.76×10^{-4} [s^{-1}]
$CO_3^- + H^+ \rightleftarrows HCO_3^-$	8.92	4.83×10^{10} [$M^{-1}s^{-1}$]	59.44 [s^{-1}]
$HCO_3^- + OH^- \rightleftarrows CO_3^- + H_2O$	/	5.79×10^{6} [M^{-1} s^{-1}]	3.06×10^{5} [s^{-1}]
$H_2O \rightleftarrows OH^- + H^+$	13.22	1.45×10^{3} [M s^{-1}]	2.23×10^{10} [M s^{-1}]

Table S1: Bulk reaction equilibrium coefficients and rate constants

Nominal reaction timescales for DIC interconversion calculated by Zeebe et. al. are order 10^{-7}s for interconversion between carbonate and bicarbonate and for water auto-ionization/recombination, but order 10s for interconversion between bicarbonate and carbon dioxide. Bulk reaction phenomena can only be resolved with timesteps on the order of the fastest reaction – therefore, kinetic constants in both directions for carbonate to bicarbonate were slowed by a factor of 10^7 to order 1s – preserving two distinct timescales separated by an order of magnitude while maintaining the overall equilibrium and enabling the solver to progress in reasonable timesteps. Water

dissociation and recombination is set implicitly by COMSOL to enforce the electroneutrality condition, and therefore did not require adjustment as a rate-limited reaction.

Due to ionic interactions, dissolved inorganic carbon speciation differs between true seawater and the laboratory-simulated seawater (sodium chloride and sodium bicarbonate). Equilibrium molar speciations for a pH of 8.1 are tabulated below:

Species	DIC Fraction (Seawater)	DIC Fraction (1.76mM $NaHCO_3$ +0.5M NaCl)
CO_3^{2-}	0.127	0.43
HCO_3^-	0.875	0.56
CO_2	0.005	0.01

Table S2: molar DIC speciation fractions in true seawater and the simulated seawater used in the experimental study described herein

Commonly reported interconversion rate constants are measured for seawater; therefore, the simulated inlet concentration of DIC was increased to approximately 2.24 mM to match the DIC speciation of actual seawater while maintaining an equal buffering capacity across both systems (here, buffering capacity is defined as $2\cdot[CO_3^{2-}] + [HCO_3^-]$). During regeneration, it is assumed that 95% of the initial DIC has been removed from the system.

Boundary conditions were formulated as electrode surfaces with Nernstian open circuit potentials (S2-S3) and current dependency governed by Butler-Volmer kinetics (S4) and a constant charge transfer resistance (S5):

$$E_{Bi} = 0.16 + \frac{RT}{nF} ln\ \frac{a_{H^+}^2}{a_{Cl^-}} = 0.16 + 0.00856\ ln \frac{a_{H^+}^2}{a_{Cl^-}} \quad \text{(S2)}$$

$$E_{Ag} = 0.23 + \frac{RT}{nF} ln\ \frac{1}{a_{Cl^-}} = 0.23 + 0.0257\ ln\ \frac{1}{a_{Cl^-}} \quad \text{(S3)}$$

$$i = i_o \left(e^{\frac{\alpha F \eta}{RT}} - e^{-\frac{(1-\alpha) F \eta}{RT}} \right) \quad \text{(S4)}$$

$$\Delta \Phi_{Ohmic} = i \cdot R \quad \text{(S5)}$$

Due to the porosity of Bi/BiOCl, cyclic voltammetry and electrochemical impedance spectroscopy measurements could not easily be fit to simple circuit models. Literature confirms a charge transfer coefficient of α=0.7 for Ag/AgCl; a value of 0.4 was assumed for Bi/BiOCl. Exchange current

densities and charge transfer resistances for the specific electrodes used in this study were fit based on cyclic voltammetry measurements and EIS spectra.

Parameter	Ag/AgCl	Bi/BiOCl
α	0.7	0.4
i_o	2 [mA/cm^2]	0.5 [mA/cm^2]
R	26.1 $\Omega \cdot cm^2$	209.4 $\Omega \cdot cm^2$

Table S3: Assumed Butler-Volmer and charge transfer parameters for the simplified electrode models

It should be noted that this simplified formulation assumes a constant exchange current density, but the thermodynamic basis of the Butler-Volmer model predicts dependence on the local activities of participating species. The model also neglects porous effects and state-dependent variations in electrode performance due to entropic effects and morphological changes between the fully oxidized and fully reduced states.

These parameters result in significant deviations in applied potentials compared to the real system: 0.28V applied yields the desired forward average current density of 0.9mA/cm^2, compared to 0.1V in the true system, while 1.07V applied is required for the same current density in the reverse reaction (compared to 0.7V in the real cell). While the overall overpotentials differ from the real system, the same average current density was achieved, suggesting reasonable predictive power for the concentration polarization phenomena of primary interest in this study.

Overall, it is likely that these parameters overestimate losses due to charge transfer while underestimating kinetic losses. The comparative sensitivity of reaction kinetics to the surface concentration of protons further underscores the importance of understanding and controlling transport phenomena when designing electrochemical swing systems for CO_2 removal.

S3. Techno-Economic Analysis

Auxiliary Systems: Similarity to Electrodialysis

Auxiliary systems such as pre-filtration, degassing, and indirect costs are not considered within the scope of the main TEA, though these costs can be reasonably estimated by reference to previous analyses for similar electrodialysis DOC systems[5-7]. Our proposed DOC system differs in the means by which acidification and alkalization is achieved, but does not meaningfully alter the nature of the acidified oceanwater. The chlorine mediation results in a negligible ~0.2% decrease in Cl^- concentration when pH is reduced to ~6, while the means for acidification (release of H^+ from H_2O) is the same as electrodialysis. Both processes have been shown to operate in the same pH ranges and at room temperature. Therefore, the downstream degassing system in an asymmetric chlorine-mediated system is expected to operate using the same methods and with similar costs as degassing techniques explored in other works. The simple membrane-less asymmetric cell system is not expected to require additional filtration when compared to membrane-based approaches.

System Parameters

The scale of our plant for Techno-Economic Analysis (TEA) is 1MT CO_2 separated per year. The plant is assumed to operate with a capacity factor of 0.9, and has renewable electricity with zero carbon footprint at its disposal of $0.03/kWh. Capital investments are levelized with a Capital Recovery Factor (CRF) of 0.082, i.e. a 6.5% discount rate and a 25 year lifetime. The present TEA focuses only on the costs associated directly with the asymmetric electrochemical cells, namely the electrochemical electricity, cell pumping costs, and cell CAPEX costs.

The Bi/AgCl electrode architecture is implemented in square parallel plate electrolyzers, each with a fixed active area (A_e) of 0.75m^2. These modular cells are placed in parallel configuration to form a stack, with one such electrode pair shown below.

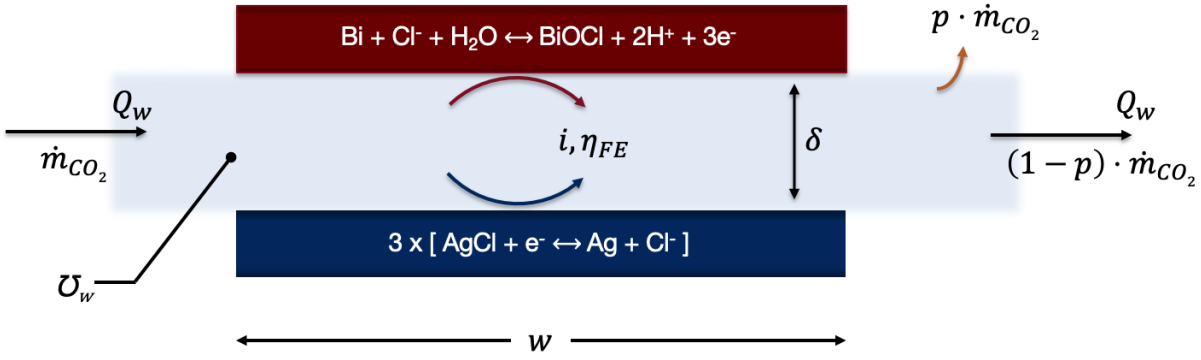

Figure S1: Oceanwater flowing between a parallel asymmetric electrode pair.

The electrochemical reaction proceeds with a geometric current density i at both electrodes and a total Faradaic Efficiency η_{FE} which is experimentally determined to be 90.4%. r denotes the ratio of electron transfer to protons transfer and is 3/2. The electrodes are spaced apart by a gap of width δ. Oceanwater with an ionic conductivity (υ_w) of 5.8 S/m flows through the gap at a flowrate denoted by Q_w. The effective mass flux of CO_2 in aqueous or carbonate ion form through the cell due to a DIC concentration of 2.4mM in the oceanwater is denoted as $\dot{m}_{CO_2}$. A CO_2 removal efficiency from the oceanwater after gas separation (p) of 87% is used from experimental results.

Electrochemical Electricity Costs

The electricity costs for operating the cell stack per tonne of CO_2 separated are calculated via equation S1, in which the first constant term is the base energy required for the reaction and the second term accounts for ohmic losses through the electrolyte.

$$C_e = \frac{\$}{kWh}\left(\frac{750\ kWh}{tCO_2} + \frac{2rF}{\eta_{FE}} \cdot \frac{i\delta}{\upsilon_w} \cdot \frac{1}{M_{CO_2}} \cdot \frac{1\ kWh}{3.6{\cdot}10^6\ J} \cdot \frac{10^6\ gCO_2}{1\ tCO_2}\right) \qquad \text{(S1)}$$

The experimentally measured 750 KWh/tCO_2 (122 kJ/molCO_2) is used for the base energy. The electrolyte ohmic loss term in equation S1 has a factor of two to account for combined losses in the acidifying and alkalizing cells. We see that this electrolyte ohmic loss becomes a significant driving overpotential at modest current densities and cell gaps, contributing 30% of the total electricity consumption at the optimized conditions of 76mA/cm^2 and an electrode gap of just 1.1mm. It should be noted that other inefficiency terms which also scale with current density such as increasing mass transport and ohmic resistances through the electrode are not included. These inefficiencies are to some extent expressed in the simplified experimental base energy term, whose magnitude cannot be readily determined for a futuristic fully developed technology. We carry forward the assumption that this value remains the same for the scaled technology as it was when experimentally determined herein. Even though the higher current densities of the deployed technology will increase some overpotentials, we expect that significant future optimization of the electrode design is possible and that similar energy requirements even at higher current densities should be attainable.

Cell Pumping Costs

In keeping the scope of the TEA to only the electrolyzer system, only the pumping required to drive the oceanwater flow through the cell stack is considered. Intake and separation pumping are generalizable to most DOC approaches and are neglected in the present analysis. The pumping costs are comprised of the capital expenditures (CAPEX) for the pump equipment and the operating costs (OPEX) of the electricity which drives the pumps.

$$C_{pump} = C_{pump,elec} + C_{pump,CAPEX}$$

The pressure drop through a single pair of square electrodes of area 0.75m^2 is calculated using a Moody diagram with a Reynolds number (Re) modified for the rectangular duct geometry formed by the square electrodes.

$$Re = \frac{\rho Q D_h}{A_{flow}\mu}; \qquad D_h = \frac{2\delta w}{\delta + w} \quad \text{(S2)}$$

Where D_h is the effective hydraulic diameter, ρ is the seawater density (1025 kg/m^3), Q is the volumetric flow rate of oceanwater, A_{flow} is the cross-sectional area of flow in the rectangular duct ($\delta \cdot w$), and μ is the viscosity of oceanwater (1.09 cP). The volumetric flow rate is calculated by matching the flux of electrons through the electrodes to the flux of CO_2 flowing through the cell in the oceanwater while accounting for the Faradaic efficiency, electron to proton ratio, and CO_2 removal efficiency as shown below.

$$Q = \frac{iA_e}{F} \cdot \frac{\eta_{FE}}{pr} \cdot \frac{1}{[CO_2]} \quad \text{(S3)}$$

A Moody diagram was used to determine the friction factor f given Re and the relative pipe roughness $\frac{\epsilon}{D_h}$. An ϵ value of 0.03mm was used after inspection of relative roughness of electrode SEM images (Fig. S3). The pressure drop across the channel was then calculated:

$$\Delta p = \frac{f\rho}{2}\left(\frac{Q}{\delta w}\right)^2 \cdot \frac{w}{D_h} \quad \text{(S4)}$$

Pumping OPEX, assumed to consist only of operational electricity costs, is calculated using a pump efficiency η_{pump} of 70%, the operation time t in seconds per year, and the number of cells required to meet the 1MT CO_2/year scale:

$$C_{pump,elec} = \frac{\$}{kWh} \cdot \frac{\Delta p Q t}{\eta_{pump}} \cdot n_{cells} \quad \text{(S5)}$$

Pump CAPEX was calculated using industrial cost estimates combined with material and pressure factors[1], yielding the bare module cost (C_{BM}), in \$/kW capacity:

$$C_{BM} = C_p^{\circ} F_{BM} = C_p^{\circ}(B_1 + B_2 F_M F_P) \quad \text{(S6)}$$

Where C_p° is \$100/kW for centrifugal pumps at powers >100kW, B_1 = 1.89, B_2 = 1.35, the material factor F_m is 2.3 for stainless steel construction, and the pressure factor F_p is 1 for moderate pressure applications. The total bare module cost, which includes direct and indirect costs, is found to be \$500/kW. The CAPEX cost is then calculated from the total pumping capacity and then levelized with the *CRF*.

$$C_{pump,CAPEX} = \frac{\$500}{kW} \cdot (\Delta P Q n_{cells}) \cdot CRF \qquad \text{(S7)}$$

In the optimized case, the electricity and CAPEX costs of pumping oceanwater through the cells total to only ~5% of the system costs. However, the higher order dependence of pumping power and energy on the electrode gap δ makes pumping costs an important consideration for cost optimization, as pumping costs grow aggressively as the electrode gap is decreased. Throughout the cases run during the optimization, a wide range of laminar and turbulent Re values were observed. The current density of the cell has a strong effect on Re, as greater flow rates are required at higher current densities to match electron and DIC fluxes. The transition to turbulence occurs around 80mA/cm^2, meaning the optimized case operating at 76mA/cm^2 is in a transitional regime. The transition to turbulence and corresponding jump in friction factor is responsible for the sudden jump in pumping costs in Figure 7b. Though turbulent flow increases pumping costs substantially, it may assist in alleviating concentration gradients and equilibrating the pH via mixing.

Cell CAPEX Costs

CAPEX costs of the electrolyzer stack are calculated by using alkaline electrolyzer cost estimates, as this technology has a similar basic architecture and has mature deployed cost estimates which are projected to reach \$300/kW[2]. The total investment cost of an electrolyzer can be broken down into three primary cost components: the power electronics (PE) required for adapting and distributing DC power, the cell stack materials and fabrication, and the balance of plant (BOP). For each of these three cost components, the costs will be adapted from the initial alkaline electrolyzer costs to arrive at an estimate for our DOC electrolyzer technology.

$$C_{cellCAPEX} = C_{PE} + C_{stack} + C_{BOP} \qquad \text{(S8)}$$

Power Electronics

Our optimized DOC plant capturing 1MT CO_2/year requires an electrochemical power (P_{DOC}) consumption of 134MW. It is assumed that power electronics costs are principally a function of the required power, and that costs per unit kW can be carried over directly from alkaline electrolyzer technology to our cell stack. At a comparative 100MW scale, power electronics account for 20% of the cost, or $60/kW.

$$C_{PE} = \frac{\$60}{kW} \cdot P_{DOC} \qquad \text{(S9)}$$

Cell Stack

Again, alkaline electrolyzer stack costs at the 100MW scale are taken as a benchmark. At this scale, the materials and fabrication of the cell stack (consisting of bipolar plates, electrodes, sealing, and structural components) constitutes the largest share of the overall investment cost at 64%. Our electro-swing DOC technology operating at cycle voltage V_{DOC} < 1V and current densities of i_{DOC} < 100mA/cm2 has a lower power density than current Alkaline electrolyzers which operate at V_{AE} ~1.8V and current densities of i_{AE} ~ 400mA/cm2[3]. Our DOC technology will therefore require a greater total geometric cell area than for our comparative alkaline electrolyzer technology.

$$\frac{A_{DOC}}{A_{AE}} = \frac{2P_{DOC}}{P_{AE}} \cdot \frac{i_{AE}V_{AE}}{i_{DOC}V_{DOC}} \qquad \text{(S10)}$$

where A_{DOC} is the total area of our DOC plant operating at a total power of P_{DOC} and A_{AE} is the total area of the benchmark alkaline electrolyzer plant operating at P_{AE} = 100MW. The factor of 2 is included to account for the combined geometric area of both the acidifying and alkalizing cell, both of which together act with a differential voltage between them of V_{DOC} and a common current i_{DOC}. In our model, cell stack costs are expected to scale with the total geometric area, as Cell Stack costs are driven largely by material requirements. The benefits of economies of scale are expected to reduce this scaling to sub-linear with a scaling factor $S_{stack} = 0.80$ for large-scale electrolyzer stacks[4].

$$C_{stack,DOC} = C_{stack,AE} \cdot \left(\frac{A_{DOC}}{A_{AE}}\right)^{S_{stack}} \quad \text{(S11)}$$

$$C_{stack,AE} = 10^5\ kW \cdot \left(\frac{\$300}{kW} \cdot 0.64\right) \quad \text{(S12)}$$

Balance of Plant

Similar to the cell stack materials, BOP costs are expected to scale proportionally to the geometric size of the cell stack, rather than the operational power. Because these components (mixers, pumps, tubing, etc) are more standardized, they enjoy a stronger cost scaling factor[4] (S_{BOP}) of 0.6. For alkaline electrolyzers at the 100MW scale, the BOP costs are 10% of the total $300/kW.

$$C_{BOP,DOC} = C_{AE,100MW}\left(\frac{A_{DOC}}{A_{AE}}\right)^{0.6} \quad \text{(S13)}$$

$$C_{AE,100MW} = 0.10 \cdot \frac{\$300}{kW} \cdot 10^5 kW = \$3\text{M} \quad \text{(S14)}$$

The power electronics, cell stack, and BOP costs are summed and levelized with a CRF of 0.082. The cell stack is the most significant cost component for all cases in the optimization study, taking an 89% share of the overall cell CAPEX costs at the optimized current density of 76mA/cm^2. The cell stack materials are the most significant cost for alkaline electrolyzer technology as well, and the lower power density and correspondingly higher required areas of the DOC electrolyzer technology push the cell stack materials to be an even larger cost driver.

However, a future more refined TEA may reveal a decrease in cell stack material costs due to looser design requirements of our DOC electrolyzer in comparison to Alkaline electrolyzer technologies. Our electrochemical swing process proceeds at lower cell voltages and more mild pH conditions, which could ease material requirements away from the specific metals which must be used for alkaline electrolyzers. Furthermore, the significantly lower optimum operational current density and lower voltage reduces heat generation effects, alleviating thermal considerations from the design. This could result in a less complex design with less total material and could even open the door to the use of much cheaper plastics as the key structural element of our electrochemical swing electrolyzer stack. These eased design requirements could lead to DOC

electrolyzer architectures which have considerably lower material costs and lower total CAPEX costs than the current predictions, making this present analysis a conservative one.

It should be noted that the cost fractions in the alkaline electrolyzer cost breakdown (power electronics, stack, BOP) do not sum to 100% because the remaining gas conditioning costs are neglected, as these costs should be part of the separation systems costs.

Our DOC technology uses Bismuth and Silver as electrochemically active materials, which are different from the catalysts used in the alkaline electrolyzer comparative technology. We assume in our analysis that the difference in catalysts will not bring a meaningful change to the system cost, as catalyst costs are typically small. For alkaline electrolyzers, the nickel anode and cathodes account for just 4% of total cost. Even for PEM electrolyzers, where precious metals (Platinum and Iridium) are used, the catalyst cost remains just 4% of the total cost[3].

Results of TEA

The present TEA was performed with similar techno-economic parameters to that of Digdaya et al. to facilitate a comparison to a bipolar membrane electrodialysis (BPMED) approach. Important parameters of the two studies are shown in Table 1.

Parameter	Value (This Work)	Value (Digdaya et al.)	Unit
TEA Parameters			
CRF	0.082	0.082	-
Lifetime	25	25	years
Discount rate	6.5%	6.5%	-
Production rate scale	1,000	~7	kt CO_2/yr
Capacity Factor	0.9	0.9	-
Electricity Cost	0.03	0.03	$/kWh
Oceanwater [DIC]	2.4	2.2	mM
Current Density	76	200	mA/cm^2
System Performance parameters			

Electrochemical Energy	122	155	kJ/molCO_2
Faradaic Efficiency	90.4%	-	-
CO_2 Removal Efficiency	87%	80%	-
Cost Estimates			
Electrochem. Electricity	$31	$37	-
Cell CAPEX	$23	$13	-
Total Electrochemical Costs	$54	$50	-

Table S1: System parameter and cost estimate comparison.

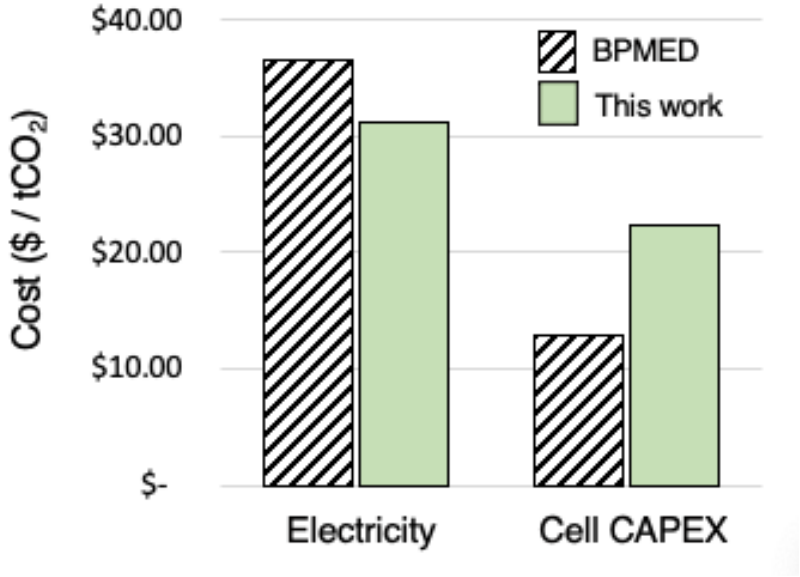

Figure S2: Comparison of projected BPMED costs (Digdaya et al.) to the costs of the asymmetric pH-swing system at optimum conditions calculated in this work. Electricity refers to only electrochemical electricity, while Cell CAPEX refers to the electrolyzer or electrodialysis cell hardware.

The electrochemical hardware (electrolyzer stack and electrodialysis equipment) and electricity costs are compared directly in Figure S2. Though different estimation strategies were used between the two studies, the cost sum is similar, at $54/tCO2 for the present asymmetric cell

approach and $50/tCO2 for the electrodialysis approach. The experimentally demonstrated low energetics of the asymmetric electrochemical pH-swing process results in a relatively lower energy cost, though estimated CAPEX is higher. Consideration of increased pumping and ohmic losses at high current densities in our model leads to the cost minimum occurring at a lower current density than that evaluated by Digdaya et al (200mA/cm^2). When evaluated at 200mA/cm^2, the cell CAPEX in this work drop by 50% to ~$11/tCO2.

The present analysis does not consider other factors such as labor, O&M, and oceanwater intake. However, the simplicity of a single compartment and absence of separating membranes is expected to keep labor and O&M costs relatively low due to reduced component count and a reduced frequency of replacement. Though this analysis focuses specifically on the costs of the electrochemical system, we emphasize the importance of addressing costs in other areas – particularly the intake and vacuum separation systems, which at present are estimated to be more significant cost drivers than the electrochemical equipment[5–7].

References

1. *Analysis, synthesis, and design of chemical processes*. (Prentice Hall, 2009).
2. DOE Technical Targets for Hydrogen Production from Electrolysis. *U.S. Department of Energy* https://www.energy.gov/eere/fuelcells/doe-technical-targets-hydrogen-production-electrolysis.
3. Emanuele Taibi, Herib Blanco, Raul Miranda, & Marcelo Carmo. Green Hydrogen Cost Reduction: Scaling Up Electrolyzers to Meet The 1.5C Climate Goal. (2020).
4. Andreas Zauner, Hans Boehm, Daniel C. Rosenfeld, & Robert Tichler. Analysis on future technology options and on techno-economic optimization. (2019).
5. Digdaya, I. A. *et al.* A direct coupled electrochemical system for capture and conversion of CO2 from oceanwater. *Nat Commun* **11**, 4412 (2020).
6. de Lannoy, C.-F. *et al.* Indirect ocean capture of atmospheric CO2: Part I. Prototype of a negative emissions technology. *International Journal of Greenhouse Gas Control* **70**, 243–253 (2018).
7. Eisaman, M. D. *et al.* Indirect ocean capture of atmospheric CO2: Part II. Understanding the cost of negative emissions. *International Journal of Greenhouse Gas Control* **70**, 254–261 (2018).